A test method for determining adhesion forces and Hamaker constants of cementitious materials using atomic force microscopy

Gilson Lomboy [a], Sriram Sundararajan [b,*], Kejin Wang [a], Shankar Subramaniam [b]

[a] Department of Civil, Construction, and Environmental Engineering, Iowa State University, Ames, Iowa 50011, United States
[b] Department of Mechanical Engineering, Iowa State University, Ames, Iowa 50011, United States

ABSTRACT

A method for determining Hamaker constant of cementitious materials is presented. The method involved sample preparation, measurement of adhesion force between the tested material and a silicon nitride probe using atomic force microscopy in dry air and in water, and calculating the Hamaker constant using appropriate contact mechanics models. The work of adhesion and Hamaker constant were computed from the pull-off forces using the Johnson–Kendall–Roberts and Derjagin–Muller–Toropov models. Reference materials with known Hamaker constants (mica, silica, calcite) and commercially available cementitious materials (Portland cement (PC), ground granulated blast furnace slag (GGBFS)) were studied. The Hamaker constants of the reference materials obtained are consistent with those published by previous researchers. The results indicate that PC has a higher Hamaker constant than GGBFS. The Hamaker constant of PC in water is close to the previously predicted value C_3S, which is attributed to short hydration time (≤ 45 min) used in this study.

© 2011 Elsevier Ltd. All rights reserved.

1. Introduction

Design of a concrete mixture with desirable workability, especially proper flow ability, is essential in every step of concrete construction, from the fresh concrete manufacturing process and quality control to the subsequent hardened concrete performance [1]. Recent advances in rheological characterization of cement-based materials have permitted engineers to formulate optimal concrete mix design and control mixture homogeneity during the concrete manufacturing and construction processes [2].

The rheological behavior of a cement-based material is primarily controlled by interparticle forces and spatial particle distribution. The interparticle forces in a flowing cement paste system consist of lubrication, adhesion, and collision forces between cement particles and/or between a cement particle and a boundary [3]. All these forces are influenced by the hydration process of cementitious materials, which depends not only upon the material characteristics (such as particle size distribution, chemical composition, water-to-cementitious material ratio (w/cm), and admixtures) but also upon the hydration time, construction process (such as mixing and placement procedures), and environmental conditions (such as time, temperature and relative humidity) [4–7]. Although a great deal of work has been done on the interparticle forces of granular and/or suspension materials, limited research is conducted to study the interparticle

forces in a cement system, which is partially due to the complexity of cement hydration [8]. Roussel et al. [9] had provided general guidelines that identify the physical microstructure parameters that govern the macroscopic rheological behavior in the steady state flow of cement suspensions. The parameters covered were interaction forces (surface, Brownian, hydrodynamic and contact forces), yield stress (particle interactions, packing and yield stress model [10,11]) and flow (shear thinning and thickening). Upon discussion of the different parameters as related to cement paste flow, a classification of different flow behaviors based on predominant interactions under simple shear with varying volume fractions and shear rates was presented.

One important parameter that depicts particle interactions is the Hamaker constant—a force constant used for describing the van der Waals force between two particles or between a particle and a substrate. Using this force constant, the particle interactions in a granular or suspension system can be simulated and predicted [9,12]. A few researchers have attempted to measure adhesion forces and Hamaker constant of cement-based materials. Uchikawa et al. determined the steric repulsive force between polished clinker and silicon in solutions with different admixtures [13]. They found that the fluidity of fresh cement pastes was correlated to the repulsive forces of their particles. Kauppi et al. measured the interaction forces between spherical and flat MgO particles using an Atomic Force Microscope (AFM) in a solution containing superplasticizer [14]. They discovered that superplasticizers contributed to both electrostatic and steric repulsion. Lesniewska et al. [15,16] evaluated the forces between calcium silicate hydrate (C-S-H) layers in different solutions. They reported that in the solution similar to

* Corresponding author.
  E-mail address: srirams@iastate.edu (S. Sundararajan).

the pore solution of a cement paste, the adhesion force between C-S-H layers was approximately 30 MPa that increased with calcium concentration. The Hamaker constant and adhesion forces of cement has also been derived by using materials that were similar to cement, as in the works of Flatt [8] and Lewis et al. [17]. Houst et al. [18] studied the action of both polycarboxylate and lignosulfonate superplasticizers on MgO powders and cement blends using microscopic and macroscopic studies and state-of-the-art techniques. Their study focused on the structure of the admixture, adsorption behavior, interfacial properties and its subsequent effect on dispersion and rheology. The atomic force microscope was used to characterize the absorbed layer thickness. Ran et al. [19] explained the effects of side chain length in comb-like copolymers on the dispersion and rheological properties in cementitious systems. It was found that a long side chain polymer had higher dispersion ability than shorter ones due to the stronger steric hindrance effect. Electrostatic repulsion and steric hindrance was responsible for dispersion in short side chain polymer.

Although the above-mentioned studies have contributed significantly to the understanding of interactions between cement particles or between cement hydration products, there is limited work on measuring the interparticle forces in a paste system containing different types of commercially available cementitious materials. There is currently no standard or commonly accepted test method for determining the interparticle forces in a cement system.

In this paper, we report a method for determining Hamaker constant of commercially available cementitious materials using Atomic Force Microscopy [20–22]. The method contains two steps: (1) measuring the adhesion force between the tested material and a selected probe using AFM and (2) calculating the Hamaker constant of the tested material from the measured adhesion force using established contact mechanics models. The adhesion force measurements are performed in both dry air and water. While performed in water, the tests are completed within 45 min after the cementitious materials contacted water. During this time period, the degree of cement hydration is limited, the cement system is mainly in a dormancy period, and the paste is still fluid or highly workable [23,24]. Thus, the interparticle forces obtained can be used for the study and simulation of cement paste rheology. The sections below present details of the method development and some preliminary results from the adhesion force measurements and modeling.

2. Adhesion force measurement

2.1. Materials

The adhesion forces between selected materials and a probe were measured using AFM. Two types of materials were selected: (1) reference materials with known Hamaker constants, used for verifying the validity of the developed test method and (2) commercially available cementitious materials, used for evaluating the application of the test method. The reference materials used were mica, silica, and calcite. Silica and calcite are commonly found in concrete as aggregate, and their Hamaker constants had been previously studied [25]. Different from silica and calcite, which have granular particles, mica has a sheet structure and is commonly used in AFM-based adhesion and friction studies [16,26–28] and can help verify the test methodology developed.

The cementitious materials used were Type I Portland cement (PC) and ground granulated blast furnace slag (GGBFS). The chemical and physical properties of the cementitious materials are given in Table 1.

2.2. Sample preparation

All materials investigated, except for mica, were in a powder form. Since mica has a thin sheet structure, it only needed to be freshly cleaved before testing. The tested material was first mixed with a two-part fast setting epoxy at a powder-to-epoxy ratio of 1:3 by weight. After mixing, the sample was placed on a glass slide and cured at 80 °C for 8 h. After cooling down, the sample was sanded flat and the surface of the sample was polished with a set of sandpapers (grits of 150, 400, 800, 1000 and 2000, from coarse to fine). During polishing, the sample was blown with pressurized line air to prevent dust accumulation. After polishing, the sample was cleaned with compressed nitrogen gas.

Fig. 1 illustrates representative 5 μm × 5 μm images of the polished samples obtained using atomic force microscopy in the standard contact mode. The roughness of the polished samples could influence the results of the adhesion force measurements. A high roughness of a sample can change the contact area and thus affect the adhesion measurements. Therefore, the root mean square (RMS) surface roughnesses of the resulting surfaces were evaluated. The RMS roughnesses of five polished materials were determined and their average RMS_{ave} are given in Fig. 1. The results indicate that the examined sample surfaces had an average RMS roughness ranging from 9.5 to 37.5 nm for a 5 μm × 5 μm scan. Among surfaces scanned, the calcite sample had the highest RMS, while PC had the least RMS values.

2.3. AFM test setup

The AFM used was the model Dimension 3100, Nanoscope IV of Veeco Instruments, CA, and the test setup is shown in Fig. 2. Standard commercially available silicon nitride (Si_3N_4) probes were used.

The AFM measurements were conducted in both dry air and water. Dry N_2 gas was used for the air environment, and Milli-Q ultrapure water was used as the water environment. When a test was performed in water, both the polished powder material and probe were completely submerged in the water.

To assess the pull-off force, normal stiffness of the probes must be known. The normal stiffness of each probe used in the present study was determined according to the method outlined by Torii et al. [29]. Two reference probes with a known normal stiffness of 0.164 and 1.28 N/m were employed. The probes used in the present study had normal stiffness ranging from 0.16 to 0.74 N/m with a deviation of 1.2% from the average.

The amount of pull-off force measured with AFM is also dependent on the geometry of the probe tip, which directly impacts the contact area. AFM probe tips have a parabolic shape and the vertex is defined by a spherical radius [30,31]. The probe tip was imaged to determine its radius with a diffraction grating TGT1 from NT-MDT, Switzerland, as shown in Fig. 3a. From the image, perpendicular sections were obtained. The image cross-section was fitted with a curve to get a radius of curvature, Fig. 3b–c. The radius of the probe tip was the average of the radius from perpendicular sections. For each probe

Table 1
Chemical components, specific gravity and Blaine fineness of PC and GGBFS.

Material	Chemical components (%)									Specific gravity	Fineness (m²/kg)
	Na_2O	MgO	Al_2O_3	SiO_2	SO_3	K_2O	CaO	Fe_2O_3	Others		
PC	0.10	3.07	4.24	21.16	2.63	0.66	64.39	3.07	0.68	3.14	452.7
GGBFS	0.29	9.63	8.54	36.5	0.60	0.44	41.1	0.83	2.07	2.95	455.0

a) Silica, RMS$_{ave}$ = 18.6nm

b) Calcite, RMS$_{ave}$ = 30.6nm

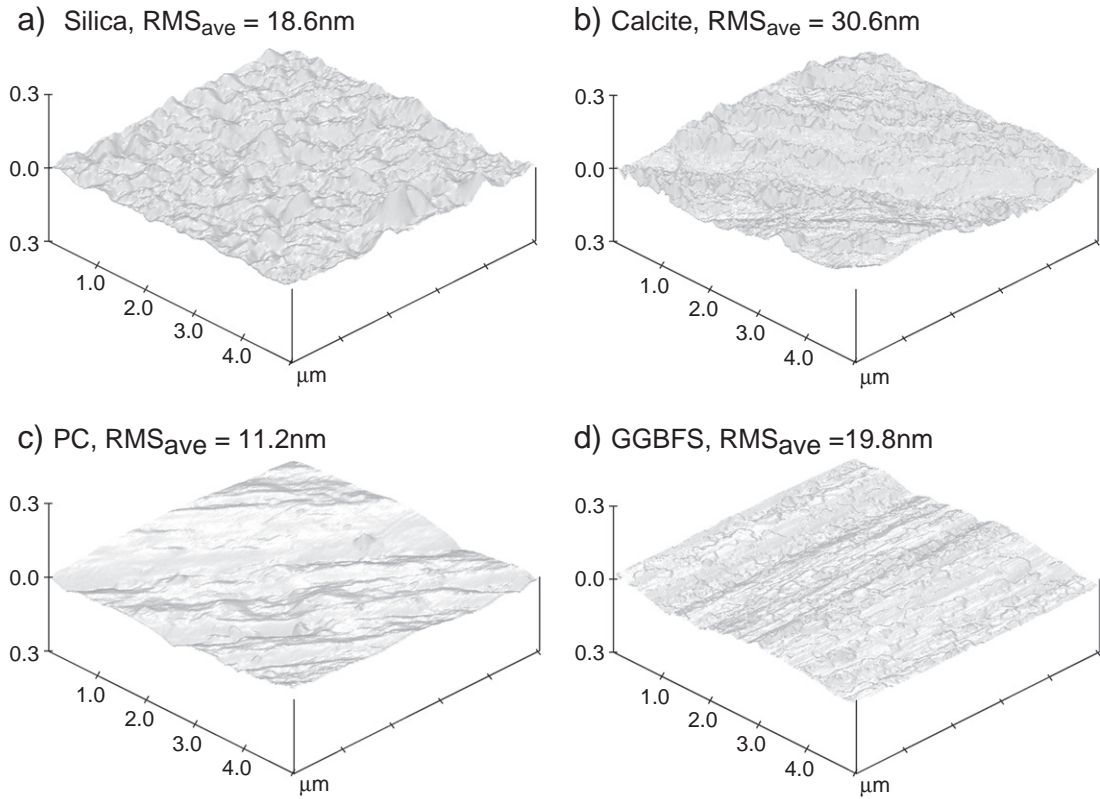c) PC, RMS$_{ave}$ = 11.2nm

d) GGBFS, RMS$_{ave}$ =19.8nm

Fig. 1. Scanned images from the surface of the sandpaper polished samples with average roughness values.

used, scans were taken from three grating tips. The variation in radius measurement for a single probe was within 13.5% of the average.

2.4. Force measurements

Force measurements are performed by acquiring force–distance curves using the AFM [32]. A schematic of a typical force–distance curve is shown in Fig. 4. In a typical measurement, the tip (at the end of the probe) is initially held far from the sample (a). It is then brought into contact with the stationary sample using a piezo-motor. As the probe approaches the sample, the attractive force gradient of the probe–sample interaction exceeds the normal spring constant at a location close to contact. This causes an instability whereby the probe tip snaps into contact with the sample and probe is seen to deflect past the "zero force" level (b). As the probe continues to advance, it presses on the sample and further deflects to its maximum value (c). Subsequently, the probe is retracted or "withdrawn" away from the sample. During this process, the probe keeps in contact with the sample (d) until the spring constant overcomes the attractive force gradient that results in the cantilever "snapping back" to its undeflected position (e). The deflection of the probe (and hence the force obtained by multiplying deflection with probe normal stiffness) is continuously recorded as a function of piezo displacement. The velocity of the probe for the whole process is 1.0×10^{-6} m/s.
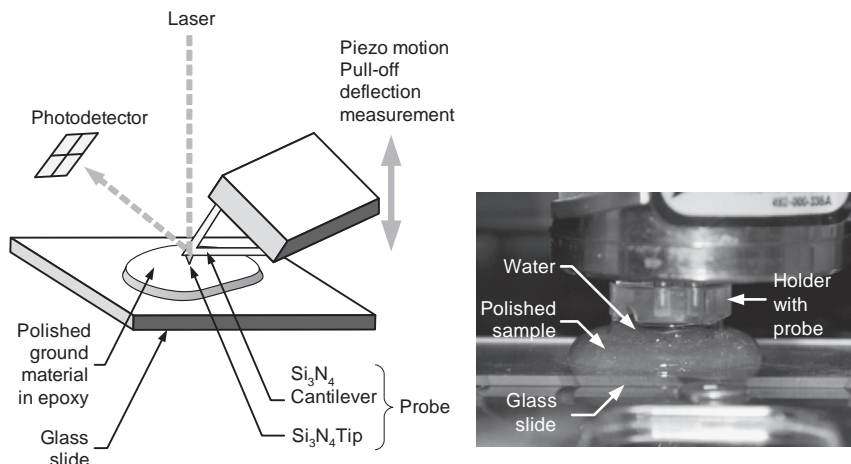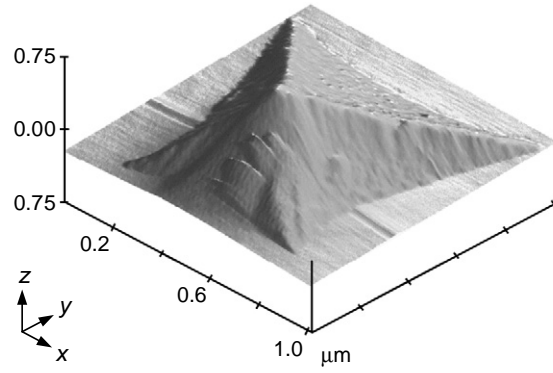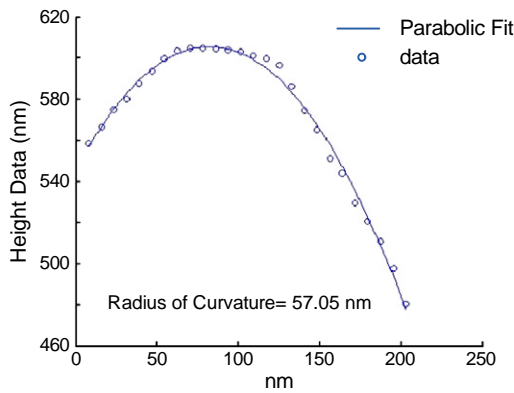
Fig. 2. Schematic of pull-off deflection measurement and setup for test in water.

a) AFM image of Si3N4 tip obtained using a tip characterization grating

b) Cross section of tip along x direction

Radius of Curvature= 57.05 nm

c) Cross section of tip along y direction
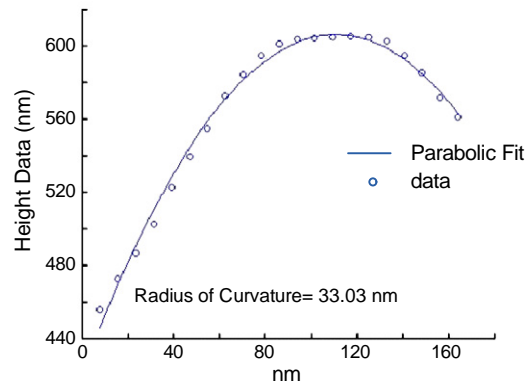

Radius of Curvature= 33.03 nm

Fig. 3. Image of Si$_3$N$_4$ tip using AFM and parabolic curve fit of tip scan data points along the x and y directions.

The pull-off force (F) between the two particles tested was calculated from the cantilever pull-off deflection (δ) and normal stiffness (k) as:

$$F = k\delta \tag{1}$$

The pull-off deflection (δ), as indicated in Fig. 4 is the distance from the initial/neutral position of the probe to the of the probe tip-sample separation.

To start the test measurements in dry air, the AFM chamber was closed and purged with N$_2$ gas to reach experimental conditions of RH≤8% to eliminate the effects of humidity on the measured forces. To test the samples in water, a droplet of water was placed on the polished sample surface. The droplet was then approached by the probe until it was fully submerged. When both the probe and polished particle were completely submerged in water, the probe approached the particle until it contacted and it was then pulled off from the particle in the same manner as the test in air.

For each material (reference or cementitious materials) tested under each environment (in air or water), five particles on a polished sample were selected. On each particle, 5 locations (1 μm apart) were chosen. For each location, 3 measurements were recorded. Thus, a total of 75 measurements were taken for each material tested under each environment condition.

2.5. Results from force measurements

All interparticle forces measured are at the nano-Newton (nN) level. Fig. 5 shows typical force curves for measurements conducted in air. The negative force corresponds to attraction and the positive force corresponds to repulsion. The slope of the repulsive region and the pull-off force varies because it depends on the properties of the contacting materials and geometry of the probe tips. Based on contact mechanics models [33,34], it is expected that as the adhesion force and the radius of the probe tip increases, the pull-off force increases.

Typical force curves for measurements conducted in water are shown in Fig. 6. The jump-to-contact between the probe and a particle was not seen in the approach curve that resulted from measurement in water. This is attributed to the double layer effects of the tested materials that typically exist in water.

As shown in Fig. 7, the double layer refers to two parallel layers of charge on the surface of the submerged particle. The first layer is a
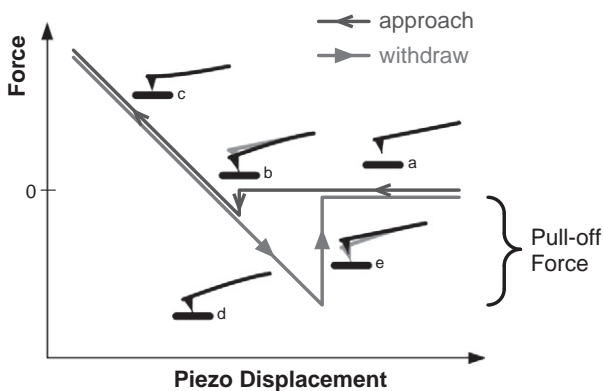

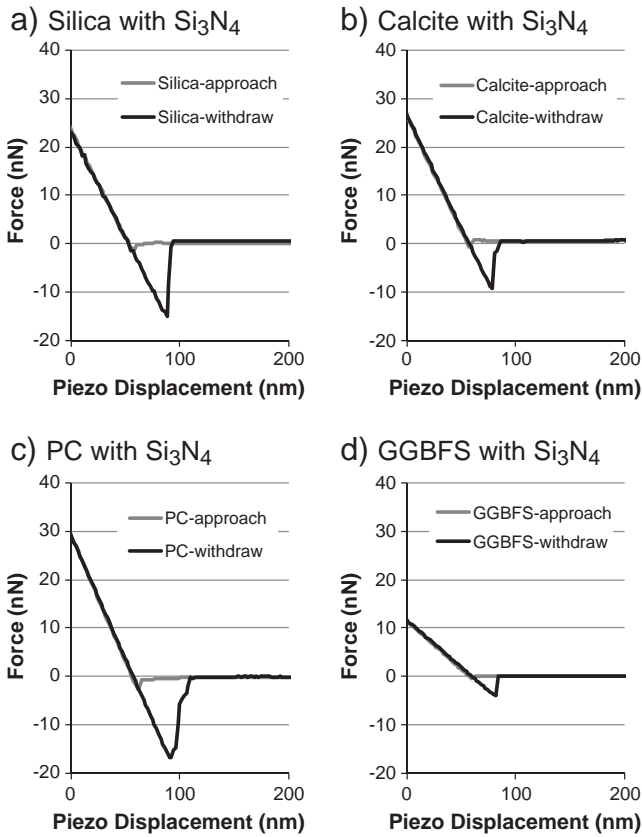Fig. 4. Sketch of a typical force curve.

Fig. 5. Typical force curves measured from tested materials and probe (Si$_3$N$_4$) in air.
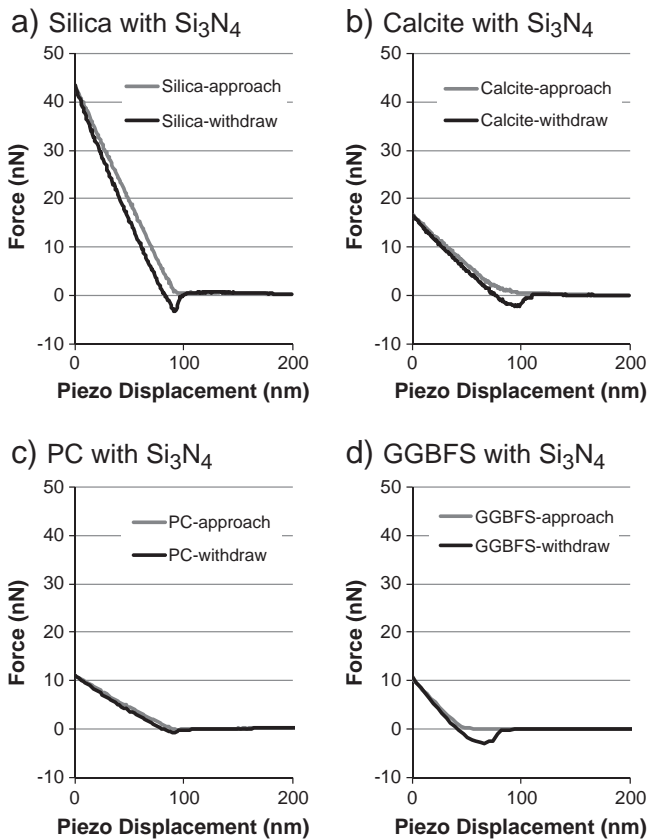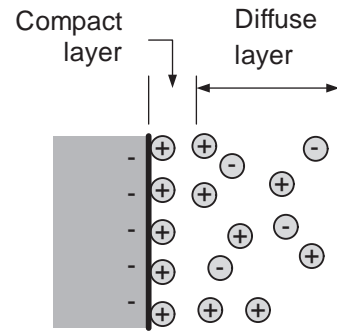

Fig. 7. Schematic of double layer formation on the surface of a submerged material.

compact layer that is made of absorbed ions due to chemical interaction. The second layer is a diffuse layer composed of ions attracted to the surface charge [35]. Because of the double layer, a repulsive force is exerted on the probe tip, which tends to reduce the jump-to-contact tendency of the probe when compared with the interaction in air.

The distribution of the calculated pull-off forces in air is shown in Fig. 8. The lines above and below the mean identify one standard deviation of the data. It is noted that PC exhibits two distinct values of pull-off forces (indicated as Group A and Group B). The force of Group A was about 56.4 nN and Group B was around 17.9 nN. As explained later, this is most likely due to the different phases in the particles of Portland cement, and the two group forces were also observed in the tests in water. Table 2 gives the mean pull-off force calculated in both air and water.

3. Hamaker constant determination

3.1. Work of adhesion

The pull-off force (F) evaluated from the experiment computed by Eq. (1) may be expressed in terms of work of adhesion (W) of the interface and AFM probe tip radius (R). Work of adhesion is the decrease in free energy per unit area when an interface is formed from two individual surfaces 1 and 2. For the purpose of this paper, the tested material will be referred to with subscript 1 and the silicon nitride probe with subscript 2. Depending on the stiffness of the material, the models by Johnson, Kendall and Roberts (JKR) [33] or by
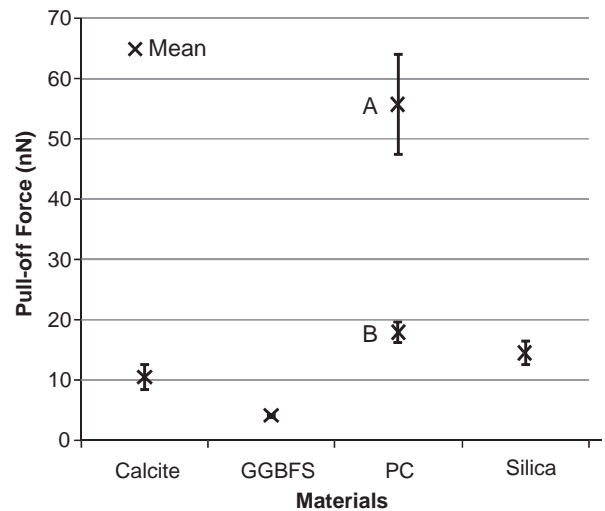

Fig. 6. Typical force curves measured from tested materials and probe (Si$_3$N$_4$).

Fig. 8. Distribution of pull-off forces for different materials tested.

Table 2
Pull-off forces of materials interacting Si_3N_4 with in air and water (nN).

Material	In air	In water
Mica	50.70 ± 0.68	
Silica	14.66 ± 0.57	2.47 ± 0.27
Calcite	10.19 ± 0.55	1.90 ± 0.46
PC (Group A)	56.42 ± 2.94	6.39 ± 2.28
(Group B)	17.91 ± 0.67	1.11 ± 0.11
GGBFS	4.06 ± 0.09	2.77 ± 0.58

Table 3
Reference material properties.

Material	E (GPa)	ν	A_{12} (×10⁻²⁰ J) Air	A_{12} (×10⁻²⁰ J) Water	μ_T Air	μ_T Water
Mica	70.7 [38]	0.25 [39]	12.8 [25]	2.45 [25]	0.20	0.07
SiO_2	72.4 [40]	0.17 [40]	10.38 [41]	1.90 [41]	0.18	0.06
$CaCO_3$	75.0 [42]	0.30[a]	12.90 [25]	2.53 [25]	0.20	0.07
Si_3N_4	280.0 [43]	0.20 [44]				

[a] Assumed value.

Derjaguin, Muller and Toporov (DMT) [35] for a spherical particle in contact with a plane surface applies. The JKR and DMT models are expressed as

$$F = c\pi R W_{12} \tag{2}$$

The constant c is 3/2 for the JKR model and is 2 for the DMT model. The work of adhesion can be expressed as a function of Hamaker constant (A_{12}) between two contacting bodies and cut-off distance (D_0). The cut-off distance is the interfacial separation between two contacting materials [36].

$$W_{12} = \frac{A_{12}}{12\pi D_0^2} \tag{3}$$

The application of the two models is usually chosen based on the Tabor parameter (μ_T) [37]. The parameter is a function of the probe tip radius, adhesion energy (γ_{12}), cut-off distance (D_0), elastic modulus of the contacting materials (E) and Poisson's ratio (ν).

$$\mu_T = \left[\frac{R \gamma_{12}^2}{E^{*2} D_0^3} \right]^{1/3} \tag{4}$$

where E^* is the equivalent elastic modulus and $E^* = E'_1 E'_2 / (E'_1 + E'_2)$ and $E' = E/(1-\nu^2)$. γ_{12} is the interfacial surface energy, $\gamma_{12} = A_{12}/(24\pi D_0^2)$. When $\mu_T > 5$, the JKR model applies, and when $\mu_T < 1$, the DMT model applies. In the present study, the average probe tip radius was 35 nm and the cut-off distance was assumed as 0.165 nm [36]. The Tabor parameters of mica, silica, and calcite interacting with a silicon nitride probe were calculated and are listed in Table 3. Since the calculated μ_T values were all much less than 1, use of DMT model is appropriate.

For the cementitious materials studied, their elastic modulus, Poisson's ratio and Hamaker constants in interaction with silicon

nitride are unknown. Thus, their μ_T values cannot be determined. Therefore, the Hamaker constants resulting from both JKR and DMT models are presented in this paper.

3.2. Random errors from experimental measurements

The Hamaker constants (A_{12}) of the materials tested with their interaction with silicon nitride can be estimated by combining Eqs. (1), (2), and (3). The resulting relations are

$$A_{12} = \frac{12D_0^2 \delta k}{cR}, \quad c = \frac{3}{2} \text{ for JKR model} \quad 2 \text{ for DMT model} \tag{5}$$

Eq. (5) illustrates that the Hamaker constant (A_{12}) is a function of four parameters (δ, k, and R) that are obtained from experimental measurements. We therefore report the Hamaker constant as

$$A_{12} = \bar{A}_{12} \pm u_A \tag{6}$$

where, $\bar{A}_{12}$ is the calculated Hamaker constant based on the mean value as expressed in Eq. (7)

$$\bar{A}_{12} = \frac{12\overline{D_0}^2 \overline{\delta k}}{c\overline{R}} \tag{7}$$

u_A is the 95% uncertainty due to combined random errors in the individual measurements.

$$u_A = \left[\left(\frac{\partial \bar{A}}{\partial D_0} u_{D_0}\right)^2 + \left(\frac{\partial \bar{A}}{\partial \delta} u_\delta\right)^2 + \left(\frac{\partial \bar{A}}{\partial k} u_k\right)^2 + \left(\frac{\partial \bar{A}}{\partial R} u_R\right)^2 \right]^{1/2} \tag{8}$$

u_{D_0}, u_δ, u_k and u_R are the individual uncertainties resulting from measurements of D_0, δ, k and R, respectively. The instrument error was calculated to be 61.0 pm [45], which is relatively small compared to random errors and are not included in the analysis.

Different values of D_0 had been reported for various materials. Plassard et al. [16] used 0.2 nm for the interaction of silica with mica, calcite or gypsum. Bhattacharya et al. suggested that D_0 for polymers might vary from 0.165 to 0.185 [46]. Matsuoka et al. reported that D_0 could be as low as 0.132 nm [47]. Israelachvilli recommended the mean value of $\overline{D_0}$ used in the calculation of interfacial surface energy as 0.165 nm [36]. Using this value, he obtained results with an accuracy of 10–20% for most materials. We therefore assume the uncertainty of D_0 as $\pm 0.10\overline{D_0}$.

As shown in Table 4 and Table 5, the uncertainty for the measurements of the pull-off deflection (δ), probe stiffness (k) and probe tip radius (R) were based on the 95% confidence interval of the measurement. The random error in the pull-off deflection was from 75 sample measurements in each material. The variation in the measurement of the cantilever stiffness was based on the data from measurements with two reference cantilevers.

Another aspect of water exposure and phase formation is the potential for changes in surface roughness. Drastic changes in roughness can significantly alter the contact area and contribute to large errors in the obtained constants. To determine the change in the surface roughness of the tested PC samples due to exposure to water, the RMS roughness of a polished PC was measured before and after

Table 4
Mean and uncertainty values of measurements in air.

	Mica	Silica	Calcite	PC (A)	PC (B)	GGBFS
δ (nm)	104.54 ± 1.40	30.23 ± 1.17	21.02 ± 1.14	116.33 ± 6.06	36.93 ± 1.38	20.29 ± 0.46
k (N/m)	0.485 ± 0.006	0.485 ± 0.006	0.485 ± 0.006	0.485 ± 0.006	0.485 ± 0.006	0.200 ± 0.002
R (nm)	76.98 ± 10.39	19.70 ± 2.66	19.70 ± 2.66	38.30 ± 5.17	38.30 ± 5.17	12.84 ± 1.73

Table 5
Mean and uncertainty values measurements in water.

	Silica	Calcite	PC (A)	PC (B)	GGBFS
δ (nm)	3.57 ± 0.395	8.02 ± 1.96	28.9 ± 10.29	5.02 ± 0.50	13.6 ± 2.86
k (N/m)	0.693 ± 0.008	0.237 ± 0.003	0.221 ± 0.003	0.221 ± 0.003	0.204 ± 0.003
R (nm)	20.60 ± 3.86	30.22 ± 2.90	36.12 ± 5.17	36.12 ± 5.17	57.88 ± 8.29

45 min of wetting. The results showed that the change is less than ± 10%. This amount of change in the surface roughness would have negligible impact on the contact area and test results. An example of a PC surface before and after wetting is shown in Fig. 9.

3.3. Hamaker constants in air

With consideration of the random errors in the experimental measurement, the Hamaker constants of the reference and cementitious materials with its interaction with silicon nitride (the probe) in air are given in Table 6.

The table shows that the values determined by the present method for reference materials studied are consistent with those published by previous researchers. Since Tabor parameter $\mu_T < 1$, only DMT model was used. The DMT model suits well for mica and silica, but it resulted in a lower Hamaker constant for calcite when compared with the value published by previous researchers. We attribute the difference to the relatively high RMS of the sample, which was 30.6 nm, while the RMS of mica, silica and cementitious materials studied were below 20 nm. The contact models assume contact between smooth surfaces. Our results suggest they provide meaningful results even for surfaces with RMS values <20 nm (5 μm scan).

Because of the two groups of pull-off forces, Table 6 shows the corresponding two values of Hamaker constants of PC. The Hamaker constant of GGBFS is lower than that of PC. The difference in the Hamaker constants' values obtained from the two models (DMT and JKR) is not significant for the cementitious materials.

3.4. Hamaker constants in water

Due to the effect of the double layer formed in the materials tested in water, a repulsive force is exerted on the probe tip. Thus, the Hamaker constant cannot be directly computed. Rather, we refer to the computed value from Eq. (6) as an "effective" Hamaker constant. Fig. 10 and Fig. 11 shows the force interaction curves [48] for tested reference and cementitious materials with Si_3N_4 probe in water with respect to the tip separation from the sample surface, respectively. It can be observed in the figure that most of the materials tested exhibited a repulsive long range force. Consistent with the results in air, PC showed two different groups of interaction curves labeled as PC (A) and PC(B). PC(A) does not have a repulsive regime that indicates a long range adhesive property.

The electric double layer on the surface of a material in water can be influenced by the ionic strength of the liquid [49,50]. For the case of calcite, its dissolution will change the ionic charge in the liquid and affect the double layer characteristics. The effects of ionic charge of the liquid on the double layer and interparticle force of commercially available cementitious materials is of interest and is part of a study currently being conducted.

The computed effective Hamaker constants in water are given in Table 7. It can be noted that the effective Hamaker constant of silica in water is still close to that reported in the previous study, while the effective Hamaker constant of calcite is much lower than that reported in the previous study. This is probably related to the relatively high dissolution of calcite in water, which enhances the double layer effect. Although much lower than those measured in air, the Hamaker constant values of PC measured in water can again be divided into two groups. The Hamaker constant values of GGBFS measured in water is also relatively lower than the reference materials. The values obtained for the two contact models (DMT and JKR) for both PC and GGBFS are not significantly different.

Energy Dispersive X-ray Spectroscopy (EDS) was employed to determine the properties of the tested sample. Fig. 12 shows the element map of polished PC with an epoxy matrix. The sample was wetted for 45 min, which was the duration of testing. The map shows the presence of different phases in the cement by the distribution of
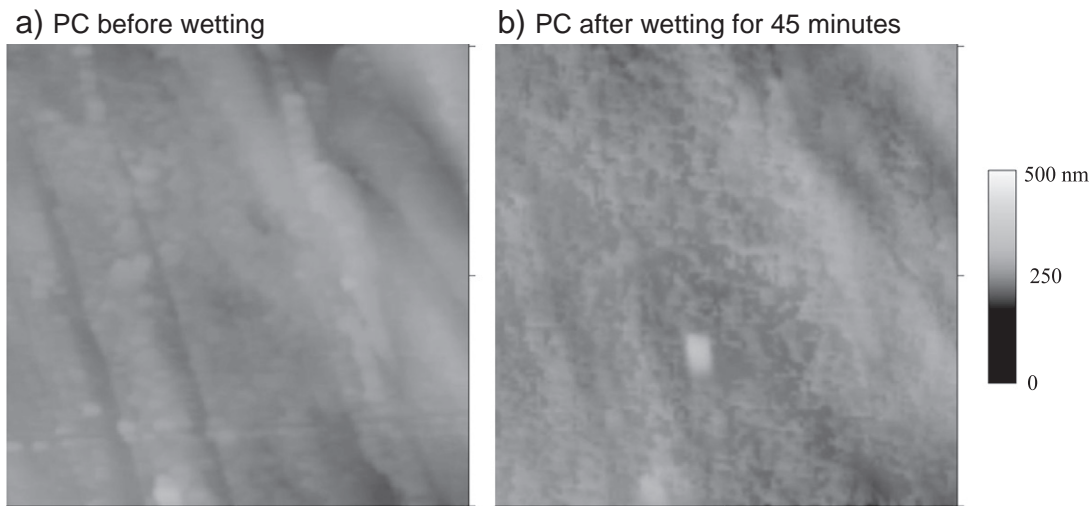

a) PC before wetting   b) PC after wetting for 45 minutes

Fig. 9. 5 × 5 μm AFM surface scan of polished Portland cement particles before and after wetting for 45 min.

Table 6
Hamaker constants A_{12} of tested materials interacting with Si_3N_4 in air ($\times 10^{-20}$ J).

Tested material	DMT	JKR	Reference
Mica	10.76 ± 2.60		12.80 [25]
Silica	12.16 ± 2.97		10.38 [41]
Calcite	8.45 ± 2.09		12.90 [25]
PC (Group A)	24.06 ± 5.95	32.08 ± 7.93	
(Group B)	7.64 ± 1.87	10.19 ± 2.49	
GGBFS	5.15 ± 1.25	6.88 ± 1.67	

calcium, silicon, aluminum and iron in the particles. Analysis of sample at different points in particles indicated the presence of unhydrated C_3S and C_2S.

In the work conducted by Flatt [8], a method of determining the approximate Hamaker constants of the different phases of partially hydrated cement in water was introduced. Based on this work, the Hamaker constants were approximately 1.6×10^{-20} J for C_3S, 0.055×10^{-20} J for ettringite, and 0.20×10^{-20} J and 0.70×10^{-20} J for C-H-S with and without nonstructural water, respectively. It is noted that the unhydrated cement compound C_3S had a much higher Hamaker constant than cement hydration products, such as ettringite.

To compare results from the present study with that from Flatt for PC in water, the Hamaker constant of PC phases can be estimated as follows:

$$A_{PC/Si3N4} = \sqrt{A_{Si3N4} A_{PC}} \tag{9}$$

Hamaker constant of silicon nitride in water (A_{Si3N4}) is equal to 4.85×10^{-20} J [25]. Taking two values of PC from Table 7 (DMT) as $A_{PC/Si3N4}$, the Hamaker constants of PC (A_{PC}) obtained from Eq. (9) are $1.72 \pm 1.49 \times 10^{-20}$ J for Group A and $0.05 \pm 0.03 \times 10^{-20}$ J and for Group B. The Hamaker constant derived from Group A is similar to the Hamaker constant estimated by Flatt for C_3S [8], which is present in the wetted sample based on the EDS analysis. This comparison further suggests that the present test method for
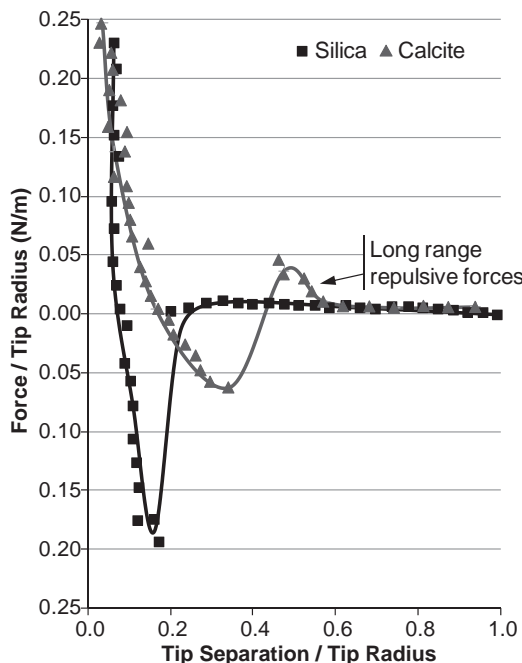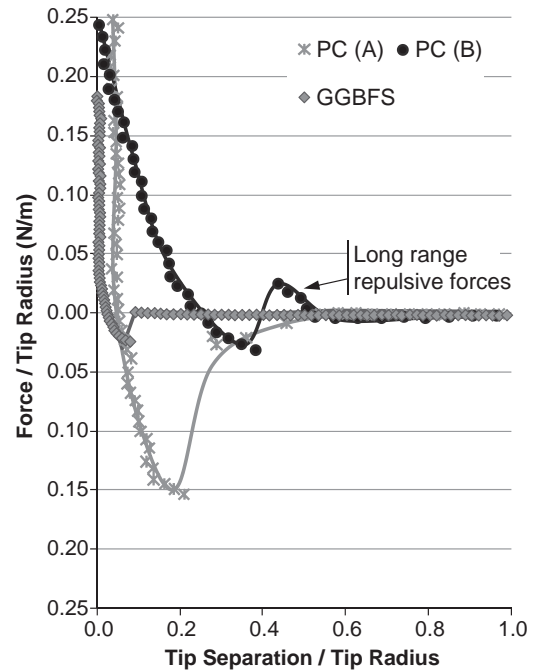

Fig. 11. Force interaction curves for tested cementitious materials with Si_3N_4 in water.

determining Hamaker constant is valid and can be used to differentiate phases in cementitious materials, provided that the difference Hamaker constant values of the phases are larger than the uncertainty values. Further examination may be needed for the Hamaker constant from Group B when considering the values from Ref. [8] and the EDS analysis. The Hamaker constant for GGBFS (A_{GGBFS}) can also be computed using the same method, and is equal to $0.12 \pm 0.09 \times 10^{-20}$ J. Because of the limit in the AFM probe stiffness and uncertainties in measurements, a lower limit may be present in the current method. These low values (less than 1×10^{-20} J) obtained from the current study need to be confirmed with further investigations.

4. Conclusions

A method for determining Hamaker constant of cementitious materials is presented. The method contains two steps (1) measuring the adhesion force between the tested material and a selected probe using atomic force microscopy (AFM) and (2) predicting Hamaker constant of the tested material based on the measured adhesion force

Fig. 10. Force interaction curves for tested reference materials with Si_3N_4 in water.

Table 7
Effective Hamaker constants of tested materials interacting with Si_3N_4 in water ($\times 10^{-20}$ J).

	DMT	JKR	Reference
From direct measurement (A_{132})[*]			
Silica	1.96 ± 0.58		1.90 [41]
Calcite	1.03 ± 0.34		2.53 [25]
PC (Group A)	2.89 ± 1.25	3.85 ± 1.67	
(Group B)	0.50 ± 0.13	0.67 ± 0.18	
GGBFS	0.78 ± 0.25	1.04 ± 0.71	
Derived with Eq. (9) (A_{131})[*]			
PC (Group A)	1.72 ± 1.49		1.60 [8]
(Group B)	0.05 ± 0.03		
GGBFS	0.12 ± 0.09		

[*] Subscripts 1, 2, 3 indicate the sample material, Si_3N_4 and water, respectively.
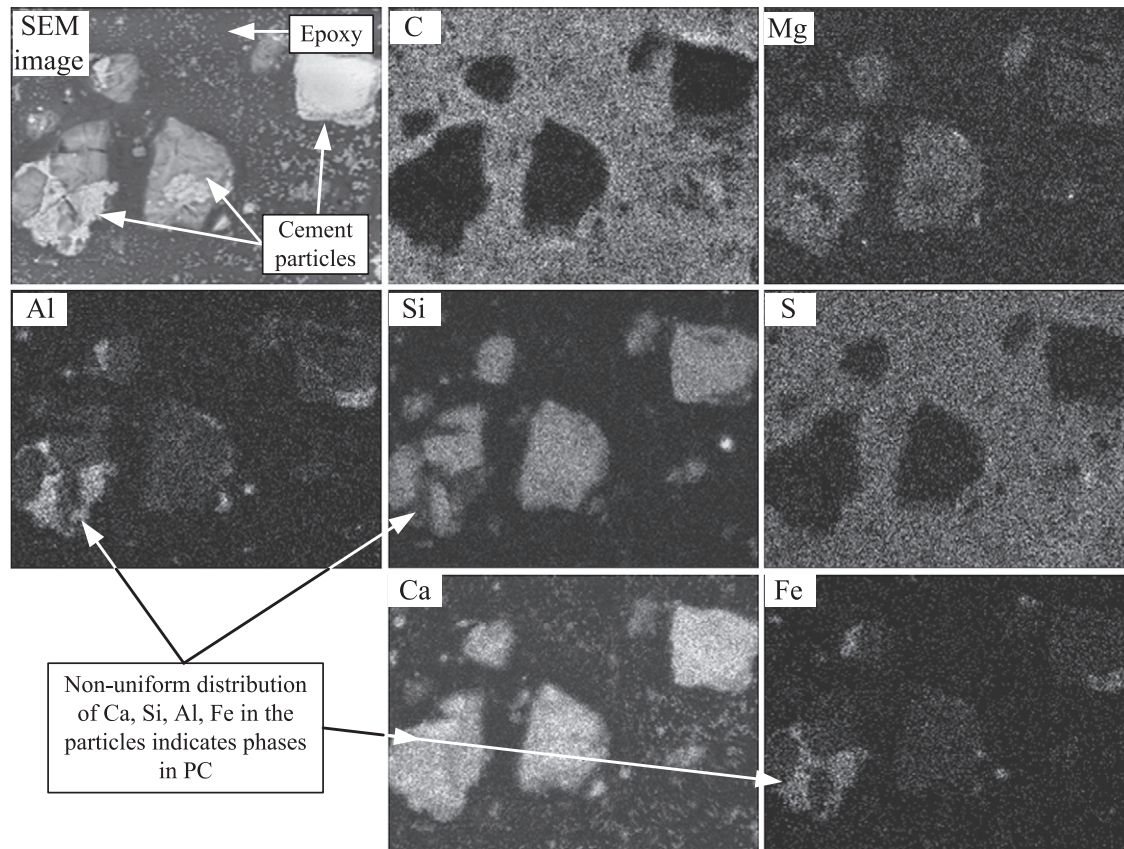
Fig. 12. Element map of polished Portland cement particles in epoxy that was wetted for 45 min (bright/dark regions indicate presence/absence of the element).

and using JKR or DMT models. The following conclusions can be drawn from the present study:

(1) Hamaker constants of the reference materials (mica, silica, and calcite) obtained from the present method are generally consistent with previously published results. This indicates that the present method is valid and reliable.

(2) Because of double layer effects, Hamaker constants of materials under a water environment cannot be directly measured. Only an effective Hamaker constant can be calculated. The effective Hamaker constants of PC and GGBFS in water are much lower than those in air.

(3) In the both air and water, the Hamaker constants of PC determined from the present study fall into two different groups, one with a high value and the other with a low value. These results may be attributed to the different phases in PC and the early-age cement hydration effect. The method has a resolution that can differentiate phases in cement. The high value of PC in water is close to the previously predicted Hamaker constant for C_3S. The application of the obtained Hamaker constant value in the study of cement system shall be further explored since the value is greatly dependent upon the phases in cement particles.

(4) Sample surface roughness can have a significant effect on the adhesion force measurement. To minimize the effect of surface roughness, it is recommended that all flat samples have an RMS less than 20 nm in a $5\ \mu m \times 5\ \mu m$ surface scan.

(5) The adhesion force measurements obtained from AFM are dependent upon the accuracy of experimental measurements for the probe stiffness, probe tip radius, pull-off deflection and cut-off distance. The random errors, or uncertainties, of these measurements should be considered in the calculation of

Hamaker constant. The estimation of a tip radius in the case of non-parabolic probe such as PC in this study is one potentially significant source of error. Another limitation of the present method in determining Hamaker constants in water is the coupling of the adhesion force and the double layer force when obtaining pull-off forces with the AFM. The double layer effects would also change with the ionic concentration in the water. As part of an ongoing study, we are currently conducting tests on different cementitious materials with varying ionic concentrations. Compared with the established methods of determining the Hamaker constants of unknown materials [25], established methods depend on the accuracy and the ability to measure dielectric properties, while the present method would be dependent on the accuracy of measuring probe stiffness, probe tip radius and pull-off deflection. However, the presented method has the advantage of being able to measure and analyze forces at a particulate level in a complex system like cement-based materials.

Acknowledgements

References

[1] G.H. Tattersall, Workability and Quality Control of Concrete, Taylor and Francis, Oxon OX14 4RN, 1991.
[2] K. Sobolev, The development of a new method for the proportioning of high-performance concrete mixtures, Cement and Concrete Composites 26 (7) (2004) 901–907.

[3] C. Crowe, M. Sommerfeld, Y. Tsuji, Multiphase Flows with Droplets and Particles, CRC Press LLC, 1998.
[4] ACI Committee 238, Report on Measurements of Workability and Rheology of Fresh Concrete, ACI 318.1R-08, American Concrete Institute, MI, 2002.
[5] T.C. Powers, The Properties of Fresh Concrete, Wiley, New York, 1968.
[6] C. Rößler, A. Eberhardt, H. Kučerová, B. Möser, Influence of hydration on the fluidity of normal Portland cement pastes, Cement and Concrete Research 38 (7) (2008) 897–906.
[7] S. Hanehara, K. Yamada, Interaction between cement and chemical admixture from the point of cement hydration, absorption behaviour of admixture, and paste rheology, Cement and Concrete Research 29 (8) (1999) 1159–1165.
[8] R.J. Flatt, Dispersion forces in cement suspensions, Cement and Concrete Research 34 (3) (2004) 399–408.
[9] N. Roussel, A. Lemaître, R.J. Flatt, P. Coussot, Steady state flow of cement suspensions: a micromechanical state of the art, Cement and Concrete Research 40 (2010) 77–84.
[10] R.J. Flatt, P. Bowen, Yodel: a yield stress model for suspensions, J. Am. Ceram. Soc. 89 (4) (2006) 1244–1256.
[11] R.J. Flatt, P. Bowen, Yield stress of multimodal powder suspensions: an extension of the YODEL (Yield Stress mODEL), J. Am. Ceram. Soc. 90 (4) (2007) 1038–1044.
[12] L. Aarons, S. Sundaresan, Shear flow of assemblies of cohesive and non-cohesive granular materials, Powder Technology 169 (2006) 10–21.
[13] H. Uchikawa, S. Hanehara, D. Sawaki, The role of steric repulsive force in the dispersion of cement particles in fresh paste prepared with organic admixture, Cement and Concrete Research 27 (1) (1997) 37–50.
[14] A. Kauppi, K.M. Andersson, L. Bergstrom, Probing the effect of superplasticizer adsorption on the surface forces using the colloidal probe AFM technique, Cement and Concrete Research 35 (1) (2005) 133–140.
[15] S. Lesko, E. Lesniewska, A. Nonat, J.C. Mutin, J.P. Goudonnet, Investigation by atomic force microscopy of forces at the origin of cement cohesion, Ultramicroscopy 86 (1–2) (2001) 11–21.
[16] C. Plassard, E. Lesniewska, I. Pochard, A. Nonat, Nanoscale experimentation investigation of particle interactions at the origin of the cohesion of cement, Langmuir 21 (2005) 7263–7270.
[17] J.A. Lewis, H. Matsuyama, G. Kirby, S. Morisette, F. Young, Poly-electrolyte effects on the rheological properties of concentrated suspensions, J. Am. Ceram. Soc. 83 (8) (2000) 1905–1913.
[18] Y.F. Houst, P. Bowen, F. Perche, A. Kauppi, P. Borget, L. Galmiche, J.F. Le Meins, F. Lafuma, R.J. Flatt, I. Schober, P.F.G. Banfill, D.S. Swift, B.O. Myrvold, B.G. Petersen, K. Reknes, Design and function of novel superplasticizers for more durable high performance concrete (Design and function of novel superplasticizers for more durable high performance concrete (superplast project)), Cement and Concrete Research 38 (2008) 1197–1209.
[19] Q. Ran, P. Somasundaran, C. Miao, J. Liu, S. Wuc, J. Shen, Effect of the length of the side chains of comb-like copolymer dispersants on dispersion and rheological properties of concentrated cement suspensions, Journal of Colloid and Interface Science 336 (2009) 624–633.
[20] S. Eichenlaub, C. Chan, S.P. Beaudoin, Hamaker constant in integrated circuit metallization, J. of Colloid and Interface Science 248 (2002) 389–397.
[21] C. Argento, R.H. French, Parametric tip model and force–distance relation for Hamaker constant determination from atomic force microscopy, J. Appl. Phys. 80 (11) (1996) 6081–6090.
[22] S. Das, P.A. Sreeram, A.K. Raychaudhuri, A method to quantitatively evaluate the Hamaker constant using the jump-to-contact effect in atomic force microscopy, Nanotechnology 18 (3) (2007) 035501.
[23] L.D. Mitchell, M. Prica, J.D. Birchall, Aspects of Portland cement hydration studied using atomic force microscopy, Journal of Materials Science 31 (1996) 4207–4212.
[24] D.D. Double, A. Hellawell, S.J. Perry, The hydration of Portland cement, Proceedings of the Royal Society of London, Series A, Mathematical and Physical Sciences 359 (1699) (1978) 435–451.
[25] L. Bergstrom, Hamaker constants of inorganic materials, Advances in Colloid and Interface Science 70 (1996) 125–169.
[26] T. Eastman, D.M. Zhu, Adhesion forces between surface-modified AFM tips and mica surface, Langmuir 12 (1996) 2859–2862.
[27] J. Hu, X. Xiao, D.F. Ogletree, M. Salmeron, Atomic scale friction and wear of mica, Surface Science 327 (1995) 358–370.
[28] R.W. Carpick, M. Salmeron, Scratching the surface: fundamental investigations of tribology with atomic force microscopy, Chemical Reviews 97 (4) (1997) 1163–1194.
[29] A. Torii, M. Sasaki, K. Hane, S. Okuma, A method for determining the spring constant of cantilevers for atomic force microscopy, Meas. Sci. Technol. 7 (1996) 179–184.

[30] D.L. Wilson, P. Dalal, K.S. Kump, W. Benard, P. Xue, R.E. Marchant, S.J. Eppell, Morphological modeling of atomic force microscopy imaging including nanostructure probes and fibrinogen molecules, J. Vac. Sci. Technol. B 14 (4) (1996) 2407–2416.
[31] R.W. Carpick, N. Agraït, D.F. Ogletree, M. Salmeron, Measurement of interfacial shear (friction) with an ultrahigh vacuum atomic force microscope, J. Vac. Sci. Technol. B 14 (2) (1996) 1289–2772.
[32] H.J. Butt, B. Cappella, M. Kappl, Force measurements with the atomic force microscope: technique, interpretation and applications, Surface Science Reports 59 (2005) 1–152.
[33] K.L. Johnson, K. Kendall, A.D. Roberts, Surface energy and the contact of elastic solids, Proc. R. Soc. Lond. A. 324 (1971) 301–313.
[34] B.V. Derjaguin, V.M. Muller, Y.P. Toporov, Effect of contact deformation on the adhesion of particles, Journal of Colloid and Interface Science 53 (2) (1975) 314–320.
[35] J. Lyklema, Fundamentals of Interface and Colloid Science, Academic Press, 2005.
[36] J. Israelachvili, Intermolecular and Surface Forces, Academic Press, Inc., San Diego, CA, 1991, p. 203.
[37] D. Tabor, The hardness of solids, J. Colloid Interface Sci. 58 (2) (1977) 145–179.
[38] L.E. McNeil, M. Grimsditch, Elastic modulus of muscovite mica, J. Phys.: Condens. Matter 5 (1993) 1681–1690.
[39] J.C. Hill, J.W. Foulk III, P.A. Klein, E.P. Chen, in: Desai, et al., (Eds.), A three-dimensional validation of crack curvature in muscovite mica, Computer Methods and Advances in Geomechanics, Balkema, Rotterdam, 2001, pp. 505–508.
[40] M. Fukuhara, A. Sanpei, High temperature-elastic moduli and internal dilational and shear frictions of fused quartz, Japanese Journal of Applied Physics 33 (1994) 2890–2893.
[41] T.J. Senden, C.J. Drummond, Surface chemistry and tip-sample interactions in atomic force microscopy, Colloids and Surfaces A: Physiocochemical and Engineering Aspects 94 (1995) 29–51.
[42] R. Gunda, A.A. Volinsky, Tip-induced calcite single crystal nanowear, Mater. Res. Soc. Symp. Proc. 1049 (2008) AA5.15.
[43] T.P. Weihs, Z. Nawaz, S.P. Jarvis, J.B. Pethica, Limits of imaging resolution for atomic force microscopy of molecules, Appl. Phys. Lett. 59 (1991) 3536.
[44] G.W.C. Kaye, Tables of physical and chemistry constants and some material functions, 13th ed. Longmana Green and Co., Ltd., London, 1966.
[45] SBO Research Technical Support, email communications, , July 12, 2010.
[46] S.N. Bhattacharya, M.R. Kamal, R.K. Gupta, Polymeric Nanocomposites: Theory and Practice, Hanser Gardner Publications, Inc., Cincinnati, Ohio, USA, 2008.
[47] H. Matsuoka, K. Ono, S. Fukui, A new evaluation method of surface energy of ultra-thin film, Microsyst Technol 16 (2010) 73–76.
[48] B. Cappella, G. Dietler, Force–distance curves by atomic force microscopy, Surface Science Reports 34 (1999) 1–104.
[49] H.G. Pendersen, L. Bergström, Forces measured between zirconia surfaces in poly (acrylic acid) solutions, J. Am. Ceram. Soc. 82 (5) (1999) 1137–1145.
[50] L. Ferrari, J. Kaufmann, F. Winnefeld, J. Plank, Interaction of cement model system with superplasticizer investigated by atomic force microscopy, zeta potential, and absorption measurements, Journal of Colloid and Interfacial Science 347 (2010) 15–24.

Glossary

$\bar{}$: bar over for mean value

1, 2, 3: subscripts pertaining to tested material, Si_3N_4 and water, respectively

A: Hamaker constant

c: contact model equation constant

D_0: cut-off distance

E: material elastic modulus

E^*: equivalent elastic modulus of contacting materials

F: pull-off deflection

k: probe stiffness

R: tip radius

u: uncertainty due to random error

W: work of adhesion

δ: pull-off deflection

γ: interfacial surface energy

ν: Poisson's ratio

μ_r: Tabor parameter